Mapping of Inundation Extent along River - Kaduna from Spaceborne Optical Sensor

AbdulAzeez ALIYU, Adamu BALA, AbdulHameed ISIAKA, Zainab ATTAH and Muhammad TIJJANI, Nigeria

Keywords: Inundation Mapping, mNDWI, River Metrics, Flow Direction, Profile and Cross-section of River.

SUMMARY

Mapping of areas inundated by flood is crucial for determining flood extent, deployment of emergency response teams, and assessment of damages and casualties. River-Kaduna, which spread over a wide area cut across certain neighborhoods, often inundates its banks predominantly during heavy rainfall, and resulting into urban flood. However, to map the extent of inundation without river gauge data is impossible. Therefore, the study presented a simple, logical and effective method of mapping the extent of the 2018 inundation along River-Kaduna. It processed two sets of Landsat OLI and TIRS images – one as pre-flood and the other as during-flood. Owing to the unavailability of river gauge data within the study area, a DEM was incorporated into the analysis to define the water level based on the derived modified Normalized Difference Water Index (mNDWI), Triangulated Irregular Network (TIN), flow direction, profile, and cross-section of the River. The study revealed that the water of the regular channel of the river before the flood covered an area of 2,748.16Km^2 with a volume of 17,804,379.17m^3. The floodwater during the flood covered 15,603.37Km^2 with a volume of 218,565,875.21m^3. The extent of the inundation was 12,855.22m^3 beyond the bank of the River and the volume of the floodwater was about 200,761,496.04m^3. Also, the flow direction of the River showed that the direction of flow of the River was 24.8% to the south direction, 24% to the west; 13.6% to the north, 11.2% to the east directions. The flow direction to south-west direction was 9.6%; followed by south-east, north-east, and north-west directions with percentages of flow of 6.4%, 5.6%, and 4.8% respectively. Some of the findings of this study are in agreement with similar related studies. This study has contributed to the techniques for mapping the extent of inundation in the absence of a river gauge data using geospatial techniques. Based on the findings of the study, it suggested that dredging of the River should be carried out to allow the it to accommodate more volume of water during heavy rainfall and allow water to flow freely through its natural channel.

Mapping of Inundation Extent along River - Kaduna from Spaceborne Optical Sensor

AbdulAzeez ALIYU, Adamu BALA, AbdulHameed ISIAKA, Zainab ATTAH and Muhammad TIJJANI, Nigeria

1. INTRODUCTION

Flood is a very high flow of water that shrouds the natural and artificial banks in any stream. The impacts (Akinola, 2015) of flood disasters on society are catastrophic and its effects on livelihood and economy can be relatively devastating. Mapping of areas inundated by flood is crucial for the determination of flood extent, deployment of emergency response teams, and appraisal of destructions and casualties (Cwik, 2017). Over time, there have been some prominent and annihilating flood incidents in Nigeria. Nigeria experienced the most damaging effects of floods in 2012. Around 13 states were affected by the flood incidents: Niger, Benue, Edo, Kogi, Anambra, Ebonyi, Ondo, Imo, Bayelsa, Delta, Rivers, Adamawa, etc. (Ejikeme, 2015). Besides, cities with waterways such as Lagos, Port Harcourt, Calabar, Uyo, Warri, Lokoja and Kaduna, and others have experienced numerous flood incidents that have annihilated many lives and properties worth millions of Naira (Ijigah and Akinyemi, 2015).

River Kaduna, which spread over a wide area or distance spans through Kaduna metropolis and cutting certain neighborhoods such as Unguwar Muazu, Tudun Wada, Kudanda, Nasarawa, Unguwar Rimi, Malali, Kigo Extention, Baban Saura, and New Millenium City, often inundates its banks predominantly during heavy rainfall resulting into fluvial flood or urban flood. Besides, the River is ungauged and majority of the structures in these neighborhoods have encroached less than 50m away from the river banks as a result of rapid urban sprawl. Prominent cases of inundation took place in August 23, 2003 (Augustine and Akinyemi, 2015); September, 2018 (Daily Trust, 2018; Premium Times, 2018; The Punch, 2018) and recently in September, 2020 (The Guardian, 2020), which annihilated essential properties.

Isma'il and Saanyol, (2013) carried out a flood vulnerability mapping along the Middle Course of River-Kaduna. They characterized the area into high risk, moderate risk, and low-risk zones. Similarly, Jeb and Aggarwal, (2008) did flood hazard modelling of the River-Kaduna using remote sensing and Geographic Information System (GIS), where flood risk maps were produced. Also, flood frequencies and different return periods of flood hazards of certain magnitudes were determined. However, no study has specifically addressed mapping the extent of the flood incidents along River Kaduna. This study, therefore, mapped the flood extent along River-Kaduna for the 2018 flood incident.

Various remote sensing techniques have been used to map flood extent both locally and internationally. The remotely sensed sensors that have been used for flood mapping are microwave and optical sensors. The former has the capability to penetrate clouds and vegetation, but the data are unavailable (if available, are expensive) and have limited historical coverage. The latter is highly available and having spatial and temporal resolutions. However, they can be limited by their inability to penetrate clouds. Though this limitation can be mitigated (Klemas, 2014) by integrating optical data with synthetic aperture radar (SAR). Wang et al. (2002) mapped flood extent by using an optical sensor (Landsat 4 and 7) and digital elevation model (DEM) to determine flooded and unflooded areas in North Carolina, USA, where the DEM was used to modelled the inundation.

Similarly, Lawrence *et al* (2005) used a microwave sensor (SAR) to determine flooded and unflooded areas in coastal Louisiana, USA. For both studies of Wang et al (2002) and Lawrence et al. (2005), two set images were used for each sensor: the first image was acquired before flooding and the second was acquired after flooding, thereby setting a cut-off value for the pixels. Schumann *et al* (2009) determined the flood extent by integrating remote sensing with hydraulic models. Ejikeme *et al* (2015) modelled the impact of flooding in Edo state using SPOT-10 image and ASTER DEM to characterized the study area into very high risk, high, moderate, low, and no risk. Lisa *et al*. (n.d) combined Sentinel 1A (C-band) and Sentinel 2B for rapid mapping of flood events in the region of Queensland Australia, which included the derivation of Normalized Difference Water Index (NDWI).

Some of the above techniques that addressed flood extent have not been able to sufficiently delineate flood extent together with its metrics, namely: surface area and volume of the flooded area. Therefore, this study aimed at mapping the flood extent of 2018 inundation along River-Kaduna to ascertain the surface area of the flooded area and volume of the inundation. The rationale in choosing the year 2018 flood incident along River-Kaduna is because it was more disastrous than 2013 and remotely sensed datasets of choice (before and during the flood) are available with minimal cloud cover. The study was achieved by the combination of Landsat (being planimetric image) and DEM (height raster) datasets. The idea of using the DEM is also to aid with the average height of the condition of the water (needed for volume computation) since the River is ungauged. The objectives of the study are: i) extract the waterbody from each Landsat image for pre-flood and during-flood, ii) derive a depth profile, cross-section, and flow direction of the River using the DEM, iii) determination of the flood extent.

The study concentrated on the middle course of the River because it is surrounded by the neighborhoods that constitute the metropolis such as Tudun Wada, Kinkino, Ungwar Muazu, Ungwar Rimi, Malali, Barnawa, Nassarawa, Kudendan, and Baban Saura (Figure 1). The findings of the study are presented in graphical and metric formats. These will serve as a tool for emergency management agencies to help in visual and mental communication, and also decision making.

2. METHODS

2.1 Description of Study Area

The study area is the middle course of River-Kaduna, which is one of the tributaries of River-Niger. Kaduna is one of the states in the north-west geopolitical regions in Nigeria. River-Kaduna is located between longitude 7°21'48"E - 7°29'36"E of the central meridian and latitude 10°27'15"N - 10°13'5"N of the equator (Figure 1). It cuts across Kaduna metropolis, which is bounded by Igabi, Kaduna north and south and comprises neighborhoods such as Tudun Wada, Kinkino, Ungwar Rimi, Malali are in the upper north of the River and neighborhoods such as Ungwar Muazu, Barnawa, Nassarawa, Kudendan are in the lower south of the River flow. At approximately (Alayande and Agunwamba, 2010) 550km long it takes its source from the Jos plateau and flows across the Kaduna plains in a northwesterly direction. River-Kaduna comprises two separate seasons: dry season which is between November and April; and wet season, which is between May and October respectively (Ismail and Saanyol, 2013). The section of the River that the study considered is 28,600km long.

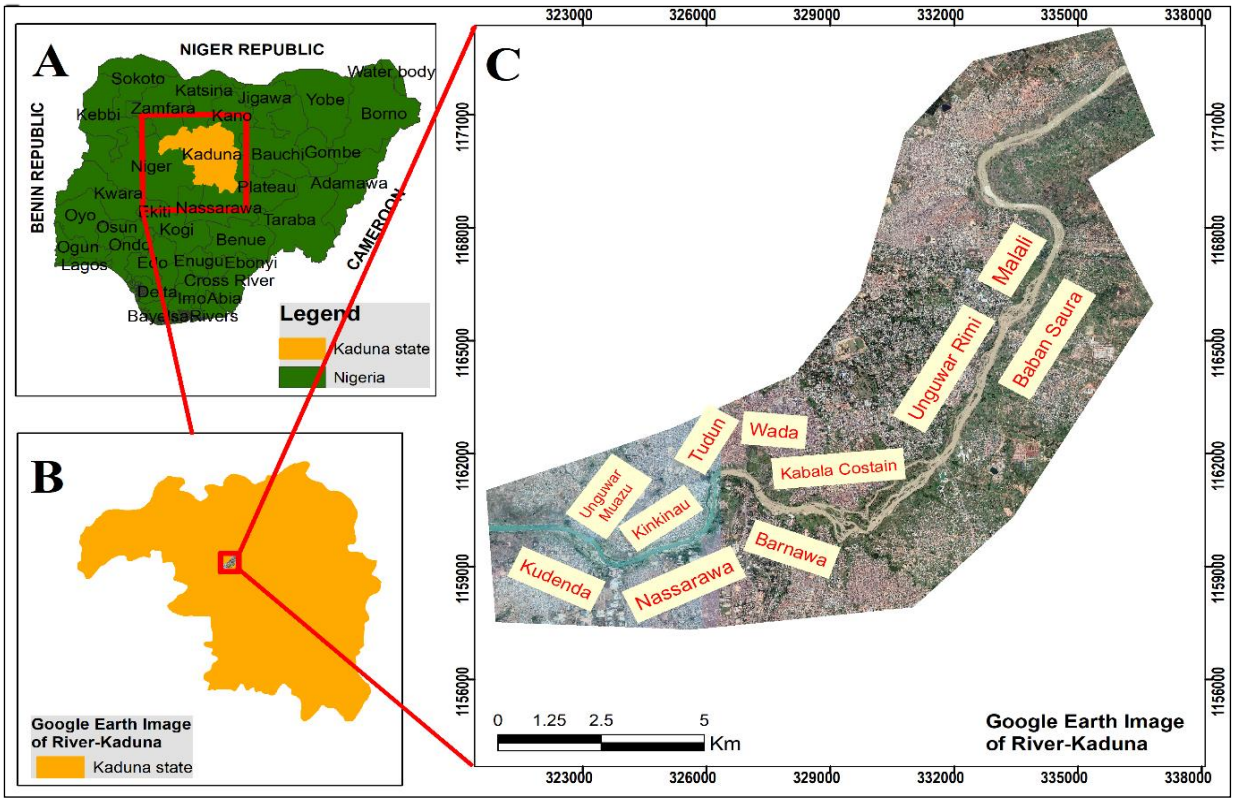

Figure 1: Inset map of the study area: (a) Nigeria (b) Kaduna state (c) River-Kaduna.

2.2 Datasets and Sources

In this study, two sets of remotely sensed images were acquired: the first image was before the flood and the second image was acquired during the flood. The former serves as reference data (Islam, n.d). The SRTM DEM has a vertical accuracy of ±16m, it is in in Geographic Coordinate System (GCS), with the World Geodetic System 1984 (WGS84) horizontal datum and Earth Gravitational Model (EGM96) geoid vertical datum (Miliaresis and Paraschou, 2005) as quoted by Elkhrachy, 2017). The details of the various datasets and their sources are shown in Table 1.

Table 1: Summary of Datasets

S/N	Data Type	Year	Cell Size	Path/Row	Source
1	Landsat OLI/TIRS	05 Mar., 2018	30m	189/53	USGS (earthexplorer)
2	Landsat OLI/TIRS	16 Sept., 2018	30m	189/53	USGS (earthexplorer)
3	SRTM DEM	Feb., 2000	30m	189/53	USGS (earthexplorer)

2.3 Data Processing and Analysis

The Landsat images were converted into the surface reflectance because most indices utilize surface reflectance as input, due to the fact that surface reflectance reflects the difference among land covers more accurately than other measurements (digital number and radiance) of remotely sensed images (Huang *et al*., 2018). The algorithms for the radiometric correction are

shown in equations 1 to 3. The techniques used in the study are encapsulated in the workflow diagram in Figure 2.

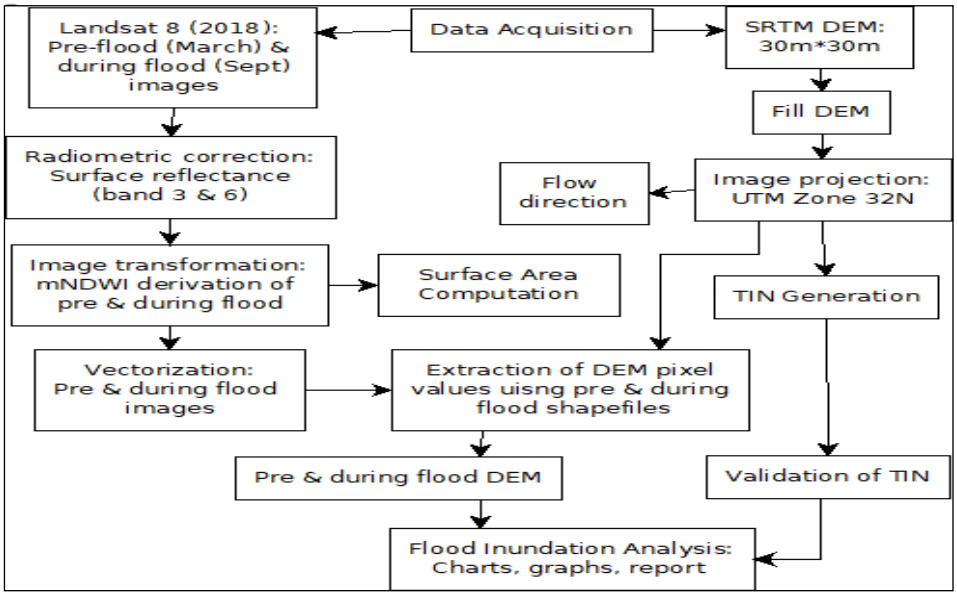

Figure 2: Workflow diagram of the study.

1. Conversion of DN to radiance (for TM and ETM+)

$$L\lambda = \frac{L_{MAX\lambda} - L_{MIN\lambda}}{Q_{calmax} - Q_{calmin}} (Q_{CAL} - Q_{CALMIN}) + L_{MIN\lambda}) \quad (1)$$

2. Conversion of DN to Radiance (green and SWIR1 only)

$$L\lambda = ML \times Qcal + AL \quad (2)$$

3. Conversion of radiance to TOA reflectance

$$\rho\lambda = \frac{\pi \times L\lambda \times d^2}{ESUN_\lambda \times COS_{SZ}} \quad (3)$$

Where: $\mathbf{L_\lambda}$ = spectral radiance at the sensor's aperture; $\mathbf{Q_{CAL}}$ = Quantized calibrated pixel value (DN); $\boldsymbol{Q_{calmin}}$ = Maximum quantized pixel value (corresponding to L_{MAXl}) in DN = 255; $\mathbf{L_{MINl}}$ = spectral radiance that is scaled to Q_{calmax} (W. m^{-1}. $ster^{-1}$. μm^{-1}); $\mathbf{L_{MAXl}}$ = Spectral radiance that is scale to Q_{calmin} (W. m^{-1}. $ster^{-1}$. μm^{-1}); $\mathbf{M_L}$ = Band-specific multiplicative rescaling factor from the metadata (RADIANCE_MULT_BAND_x, where x is the band number). $\mathbf{A_L}$ = Band-specific additive rescaling factor from the metadata (RADIANCE_MULT_BAND_x, where x is the band number); ***rl*** = unitless TOA or planetary reflectance;

$\mathbf{L_\lambda}$ = spectral radiance at the sensor's aperture; **d** = Earth-Sun distance in astronomical units from nautical handbook or interpolated values from Julian day calendar and day of the year (DOY) in excel file; $\mathbf{ESUN_l}$ = mean solar exoatmospheric spectral irradiance. $\mathbf{COS_{SZ}}$ = solar zenith angle in degrees.

SZ = 90° - Θ_{SE}, where **SE** = sun elevation [(Lathrop, 2004); (LSDS, 2019)].

Then, to obtain the surface reflectance, the Dark Object Subtraction (DOS) method as an atmospheric correction was applied to the TOA reflectance in equation (3). Here, the fundamental assumption of this method is that within the Landsat image, some pixels are dark or are in complete shadow (which are not supposed to reflect radiation) and their outgoing radiances (known as path radiance) are sensed at the sensor due to atmospheric scattering [(Chavez, 1988), (Amidon, 2014), (O'neil-Dunne, 2014), Gilmore *et al*., (2015), (GSP, 2019)]. Therefore, the darkest pixel (with the least radiance value) is subtracted from each pixel value in the image. The radiometric corrections were carried out in ENVI v5.2 and ArcGIS v10.5.

$$\text{Surface Reflectance} = \rho\lambda \times - \rho_{Dark\ Object} \quad (4)$$

Where $\rho_{Dark\ Object}$ is the darkest pixel in the image and the least reflectance value.

2.4 Image Transformation (mNDWI)

The waterbody for the months of March and September in the Landsat 8 images were extracted by deriving Modified Normalized Water Index (mNDWI). The extracted waterbody for March corresponds to pre-flood, which is the regular river channel, and the extracted waterbody for September is the during-flood. Yang and Chen (2017) expressed that mNDWI may be used when interested in urban flooding. It ranges from -1.0 to 1.0 and it is expressed as follows (Xu, 2006):

$$\text{mNDWI} = \frac{band\ 3 - band\ 6}{band\ 3 + band\ 6} \quad (5)$$

Where bands 3 and 6 correspond to green and $SWIR_1$ bands. The expression for the water index was computed using the raster calculator tool in ArcGIS v10.5. Thus, the extracted waterbody for both images was reclassified, vectorized, and clipped.

2.5 Generation of TIN, Profile, Cross-section, and Flow Direction

Since there exist no river gauge reading in the study area during the 2018 flood, which is highly required to reconstruct the 2018 flood level. Thus, there was a need to make use of a DEM and it was clipped to exactly to the River course for both the pre-flood (March) and during-flood (September). Therefore, the extents of the extracted waterbodies for the pre-flood (March) and the during-flood (September) were used. Thus, the void in the DEM image was filled using elevation void fill function. The function (ArcGIS, 2016) uses the plane fitting/Inverse Distance Weighted void fill method, where the average of the eight neighboring values are calculated to fill small voids, then the plane fitting method is applied. If the error of the plane fitting method is too large, an IDW is algorithm is applied. The elevation void fill function is in the image analysis tool in ArcGIS v10.5.

Then, the pre-flood and during-flood mNDWI images were overlaid on the filled DEM to extract the corresponding DEM height values based on the extent of the mNDWI. The mNDWI images overlaid on the DEM were examined and threshold values were selected to mask out the DEM values for the extent of the pre-flood and during-flood. This was achieved using a conditional statement tool in the spatial analyst toolset in ArcGIS v10.5. The lowest height values for both the pre-flood and during-flood is 571m, while the highest value for the former is 590m and 594m for the latter as shown in Figure 3. Therefore, the flood level was

571m above mean sea level (reference to the Earth Gravitational Model (EGM96) geoid vertical datum. The 571m value is close to the value (572.91m) used by Alayade and Agunwamba (2010), who used an eye witness account and interview made during the field survey in their work.

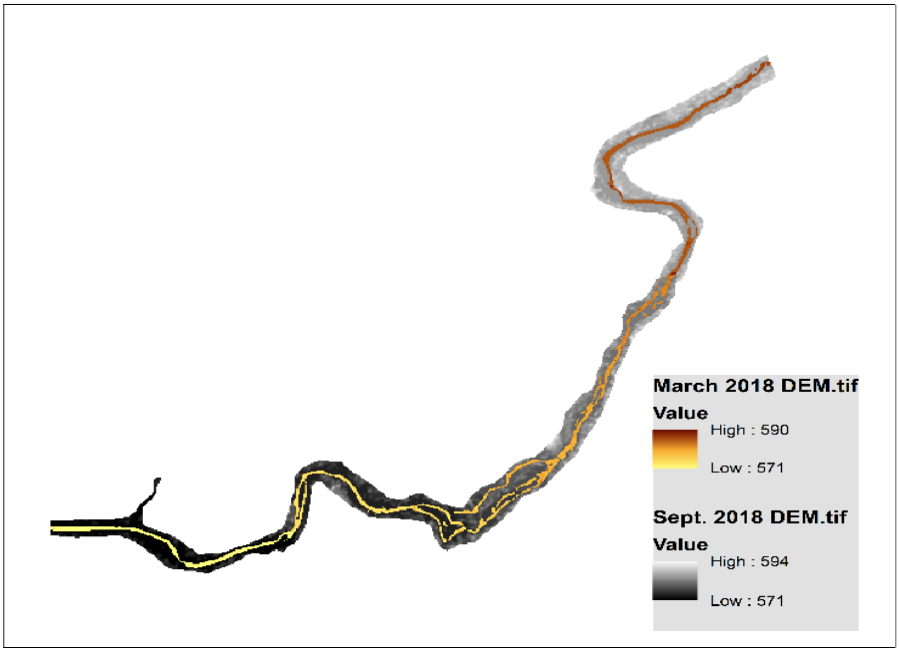

Figure 3: Inundated DEM based on the extent of pre-flood and during-flood.

More so, a Triangular Irregular Network (TIN) was generated for the during-flood of the River. The TIN was used to derive profiles of the before-flood and during-flood starting from 0m to 28,600m along the course of the River. The cross-sections were derived at intervals of 9,533m i.e. 0m, 9,533m, 19,066m, and 28,600m respectively along the course of the River. The profile and cross-sections were done using the 3D spatial analyst tool. To ascertain the flow direction of the River, a flow direction was also derived for the during-flood using the hydrology toolsets in ArcGIS.

2.6 TIN Validation

Statistical computation and visual analysis were used for the validation of the vertical accuracy of the TIN (interpolated surface). Though there was unavailability of Ground Control Points (GCPs) within the study area. Therefore, the study used the SRTM DEM points as reference points since the SRTM DEM is a systematic grid of cells at 30m interval. The DEM was converted to points and 500 points were randomly selected from the DEM and were used as reference elevations. The raster to points tool in ArcGIS v10.5 was used for the conversion.

Then, the extracted 500 reference points were overlaid on the TIN and the coincided elevation values of the TIN surface were extracted onto a separate field of the 500 sample points. The add surface information tool in 3D analyst toolsets in ArcGIS v10.5 was used for the task, which extract attributes features with spatial information derived from a surface.

Mean Absolute Error (MAE) (Habib et al., 2020), Root Mean Square Error (RMSE) (Elkhrachy, 2017) and standard deviation were used for the statistical evaluation as shown in equations 6, 7 and 8. The MAE measures the absolute deviation of the interpolated values. A value of zero indicates perfect agreement and greater than zero an average fraction of the discrepancy normalized to the mean (Isioye, et al., 2015). The standard deviation measures the dispersion of the interpolated values from the mean, the RMSE measures the average square error with values near zero indicating a close match and it sums (Elkhrachy, 2017) sums them into a single measure of predictive power.

$$\text{MAE} = \frac{1}{N}\sum_{i=1}^{n} |\Delta z_{(i)}| \quad (6)$$

$$\text{RMSE} = \sqrt{\frac{1}{N}\sum_{i=1}^{n} (\Delta z_{(i)})^2} \quad (7)$$

$$\text{StDev} = \sqrt{\frac{1}{N-1}\sum_{i=1}^{n} (z_{(i)} - z_{mean})^2} \quad (8)$$

Where N is the sample points, Z_{mean} is the mean value of the elevations, $\Delta z_{(i)}$ is the residuals of the reference elevations and the interpolated elevations.

2.7 Surface Area and Volume

The surface area of the pre-flood and during-flood was computed using equation 9.

$$\text{Surface Area} = \text{pixel size} \times \text{pixel count} \quad (9)$$

To compute the volume, the pre-flood and during-flood DEM images were used. Thus, the logic is that for the DEM image of pre-flood and during-flood, the highest pixel value (water level) and the height values below it were considered wet pixels i.e. 590 and below for pre-flood and 594 and below for during-flood (Figure 4).

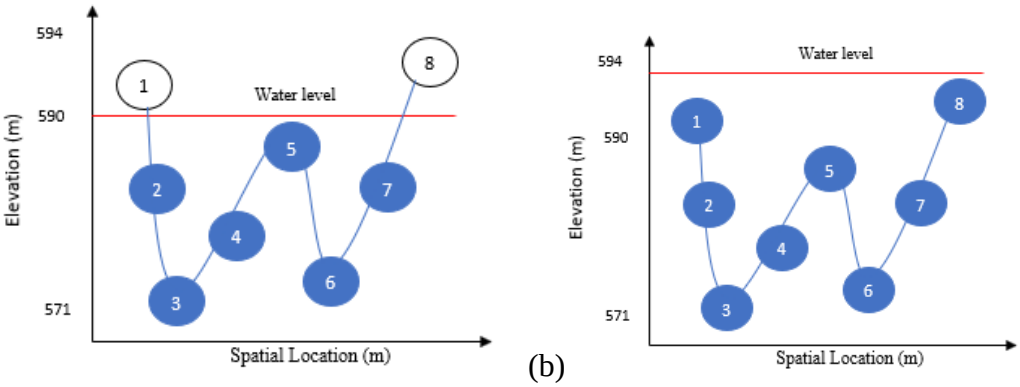

Figure 4: Elevation of the waterbody. (a) Pre-flood (March). (b) During-flood (September).

From Figure 4, the dry pixels are in white while the wet ones are in blue. The water level is considered the reference plane, which is the plane height and is set to "below" in the surface

volume tool in 3D analyst toolsets. This means that the volume was computed from the reference plane down to the lowest pixel (height) value. The flood extent is the difference between the pre-flood and during-flood as shown in equations 10 and 11.

$$\text{Flood Extent} = \text{Surface area (during} - \text{flood)} - \text{surface area (pre} - \text{flood)} \quad (10)$$

$$\text{Flood Extent} = \text{Volume (during} - \text{flood)} - \text{Volume (pre} - \text{flood)} \quad (11)$$

3. RESULTS AND DISCUSSION

3.1 Extracted Waterbody

The extracted waterbody image maps for the pre-flood and during-flood are presented in Figure 5. The mNDWI ranges from -1 to 1. Waterbody has higher positive values and are represented in white color, while non-water features (soil, vegetation, and built-up) have lower negative values and are shown in grey to black colors (Figure 5). This is because waterbody generally engross more SWIR energy than NIR, and the non-water features reflect more SWIR energy than green (Xu, 2006). The extracted waterbody delineates the meander and shape of the River. From visual inspection, the pre-flood image was narrower than the during-flood image. This means that the River increased in size during the flooded month. Their sizes are presented in the subsequent section (Table 3).

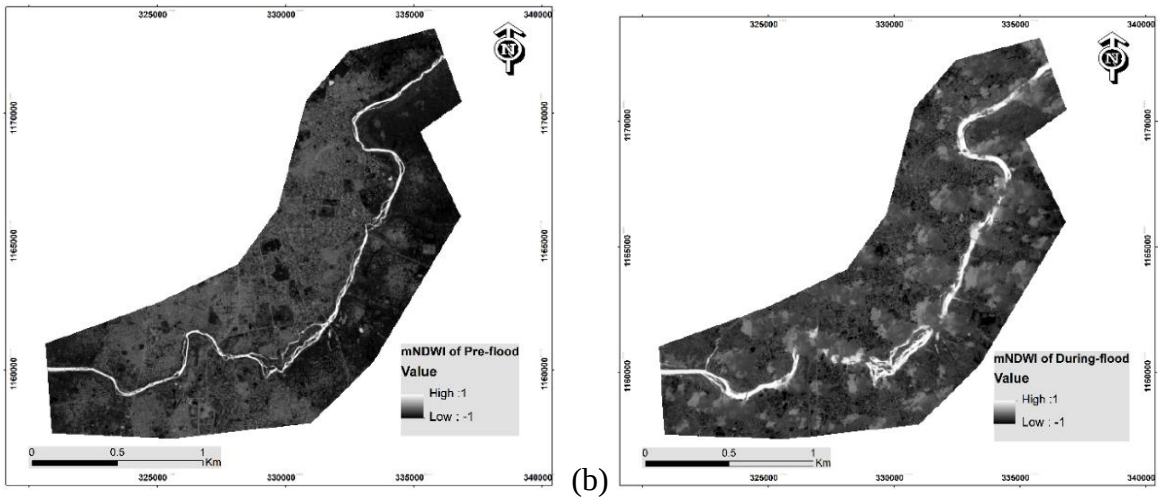

(a) (b)

Figure 5: mNDWI of River-Kaduna. (a) Pre – flood (b) During – flood.

3.2 TIN, Flow Direction, Profile, and Cross-section

The TIN, flow direction, profile, and the cross-section of River-Kaduna are shown in Figures 6, 7, 8, and 9 respectively. Figure 6 shows the interpolated surface (TIN) of the River and its vicinity, which depicts the configuration of the terrain at certain elevation and their corresponding colors. At the starting point, 0m (chainage 0+00) along the River course, the River is on high ground as shown in light blue. The lowest point is at chainage 28,600m (28+600) and is displayed in dark blue. The higher ground in the vicinity of the River is generally on a high elevation and increases further away from the bank of the River. This infers

that the lowest points are on the River course. This conforms to the fact that water flows due to gravity i.e. from higher to lower ground.

The flow direction of the River overlaid on the during-flood image and on the Google image is shown in Figure 7. The percentage of the cardinal directions is presented in Figure 8. The flow direction depicts the cardinal direction (north, south, east, west, etc.) of the River. Here, the axiom is that water flows from an elevated point to a low point as depicted by the TIN (Figure 6). However, during the inundation, water counter this fact i.e. from a low point to a high point. The percentage of the flow direction of the River is shown in Figure 8. The direction of flow of the River was mainly 24.8% to the south and 24% to the west directions. The flow direction to the south-west and north-east directions were 9.6% and 6.4%. The south and south-west directions of the flow of the River were towards Kudenda, Nassarawa, and Barnawa neighborhoods. The north and north-west directions were towards Tudun Wada, Kinkinau, Unguwar Muazu, and Kabala Constain neighborhoods. The north-east direction was towards Unguwar, Rimi, Malali, and Kigo Extension. The above result implies that settlements in the south direction are highly susceptible to inundation. The west direction signifies the continuity of the flow of the River. Settlements in the north and north-east directions were also highly susceptible to inundation. Therefore, the flow direction delineates the direction of flow of the River to contiguous settlements. This is corroborated by the works of Ismail and Sanyol (2005) and Jeb and Aggarwal (2008), which classified these neighborhoods as high risk to flood vulnerability.

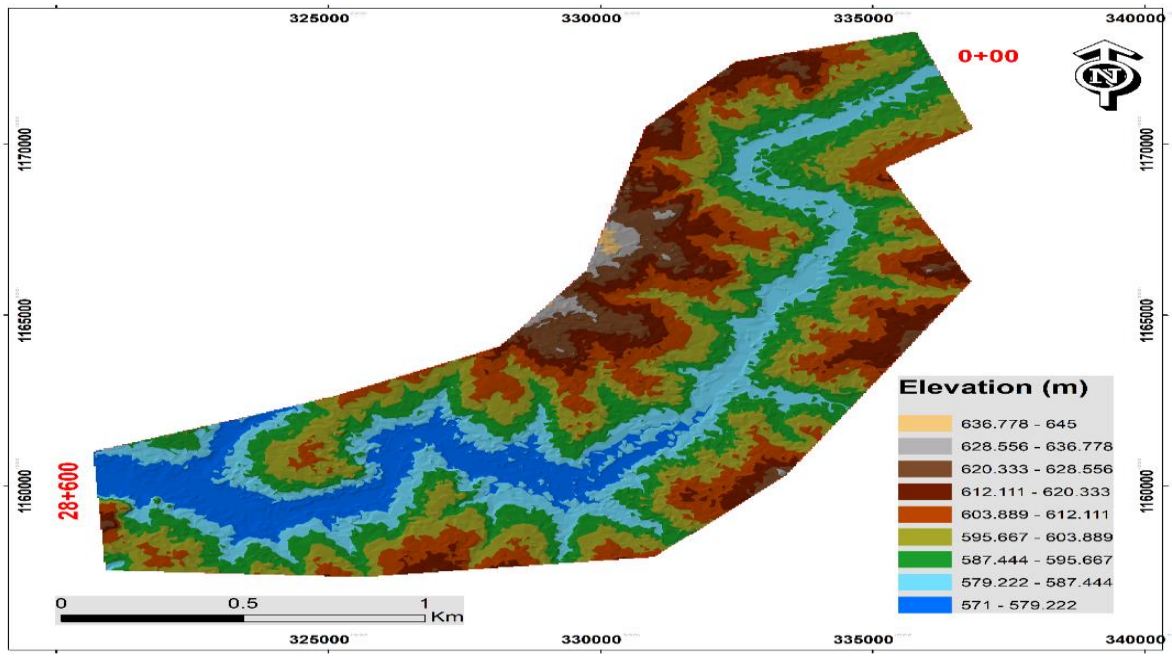

Figure 6: TIN map of "during – flood" of River-Kaduna.

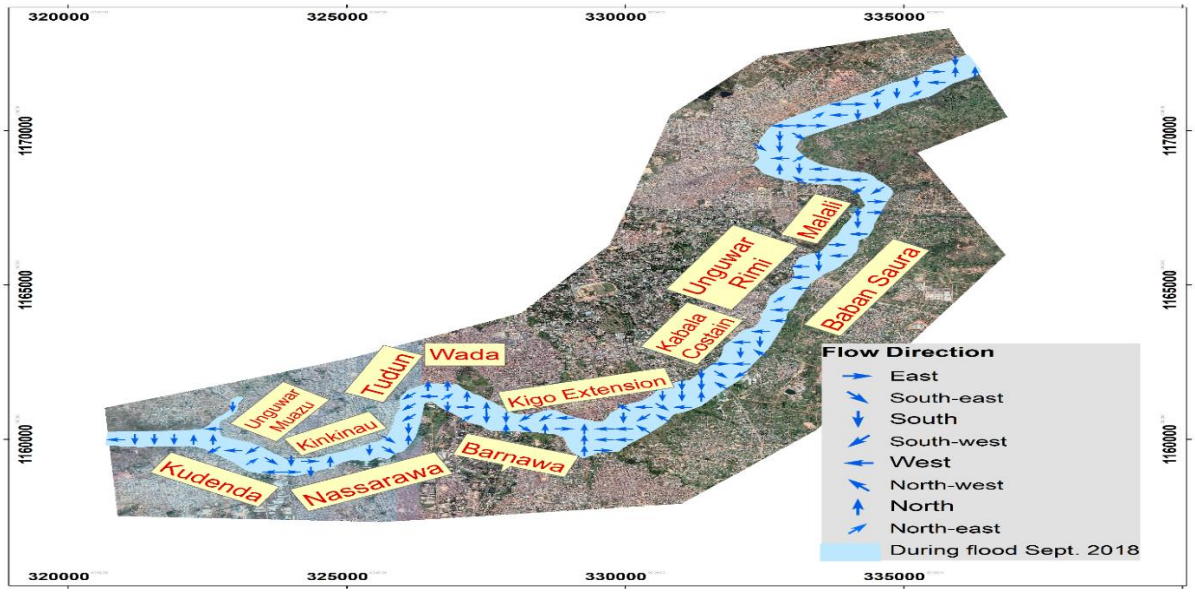

Figure 7: Flow direction of the during-flood (September 2018) of River-Kaduna overlaid on Google image.

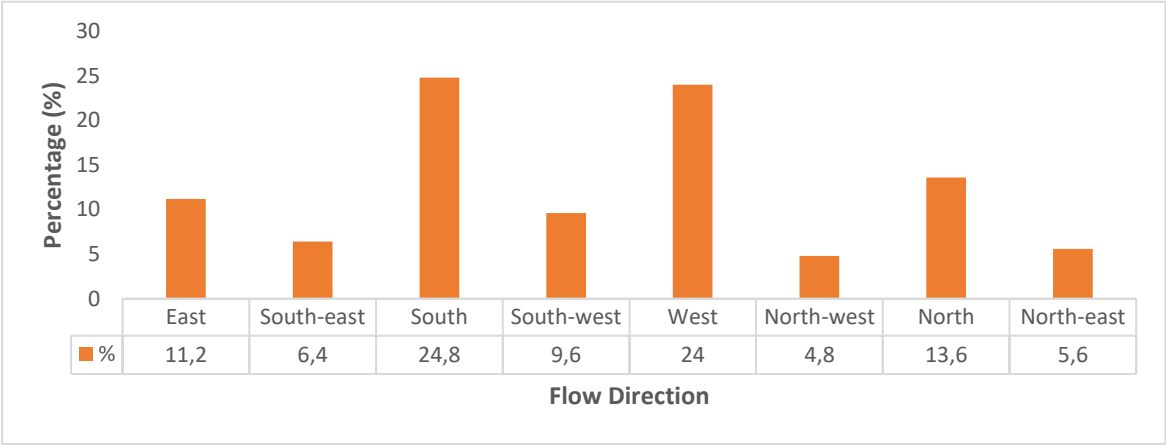

Figure 8: Percentage of the flow direction of during-flood (September 2018) of River-Kaduna.

To further investigate the vertical section of the River, Figure 9 shows the profile of the River. The profile highlights the crest and sag, and the straight lines connecting them along the centerline of the River. There was flat ground from 0m to 2000m, then a drop at 2000m. The River remains flat from 2000m to 9000m with a small crest at 5000m. There was a continuous drop in height all through from 5000m to 17000m but with short spikes or bumps (crest) in-between. The ending of the River was a flat run with short spikes. These spikes are as a result of rock-outcrops that are within the path of the River.

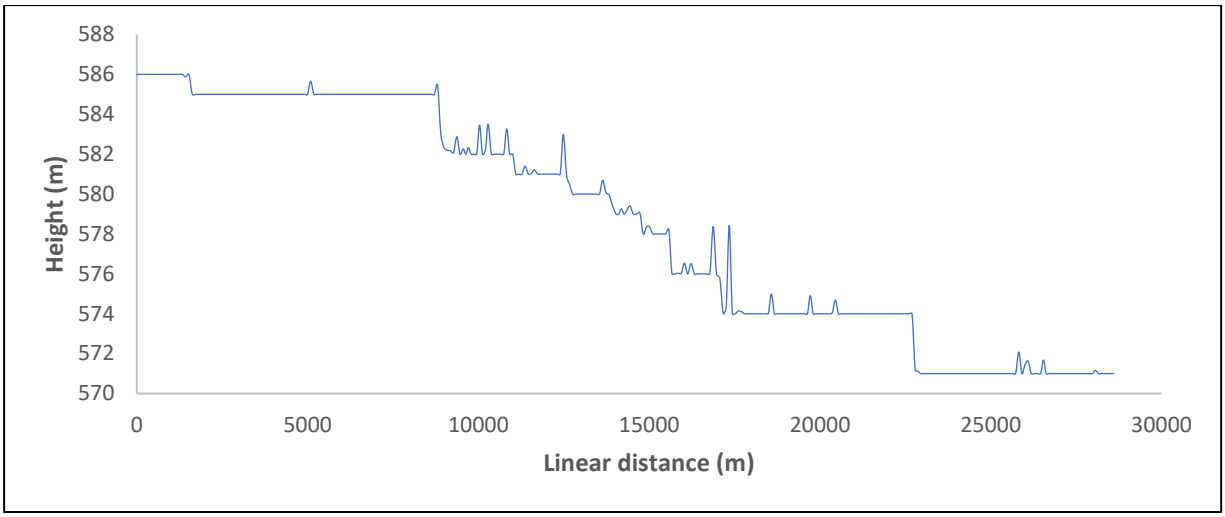

Figure 9: Profile of River-Kaduna from chainage 0m (0+00) to chainage 28,600m (28+600).

More so, the result of the profile of the River was corroborated by the cross-sections, which is at intervals of 9,533m along the River course. It delineates the heights of the right and left banks of the River. Figure (10a) shows the cross-section at 0m (0+00) and the bottom of the River was at a height of 586m amsl. The right bank was 594.04m and the left bank was 590.36m. Also, at 9,533m (9+533), the bottom was 582m, and the right and left banks were 585.06m and 587m (Figure 10b). At 19,066m (19+066), the bottom was 574m, and the right and left banks were 575.38m and 576.19m (Figure 10c). Lastly, at 28,600m (28+600), the bottom was 571m, and the left and right banks were 575.6m and 583.49m (Figure 10d) respectively. This confirms that the path of flow of the River was lower than the higher ground in the vicinity of the River. It also delineates the water depth (i.e. water-surface to the ground) before the floodwaters overtop the channel banks and spread out. Importantly, this result implies that at 0m (0+00), the right bank was higher than the left bank. Thus, neighborhoods to the right bank were not prone to inundation of the River and vice versa. More so, along chainages 9+533, 19+066, and 26+600, the right bank was lower than the left bank. Therefore, neighborhoods on the right-hand side of the River (Malali, Unguwar Rimi, Kabala, Constain, Kigo Extension, Tudun Wada, Kinkinau, and Unguwar Muazu) are highly susceptible to flooding (see Figure 7). This finding agrees with the study of Alayade and Agunwamba (2010), which identified Ungwan Rimi, Kabala Doki and Kigo road extension as the most critical areas where the right banks are lower than the left banks.

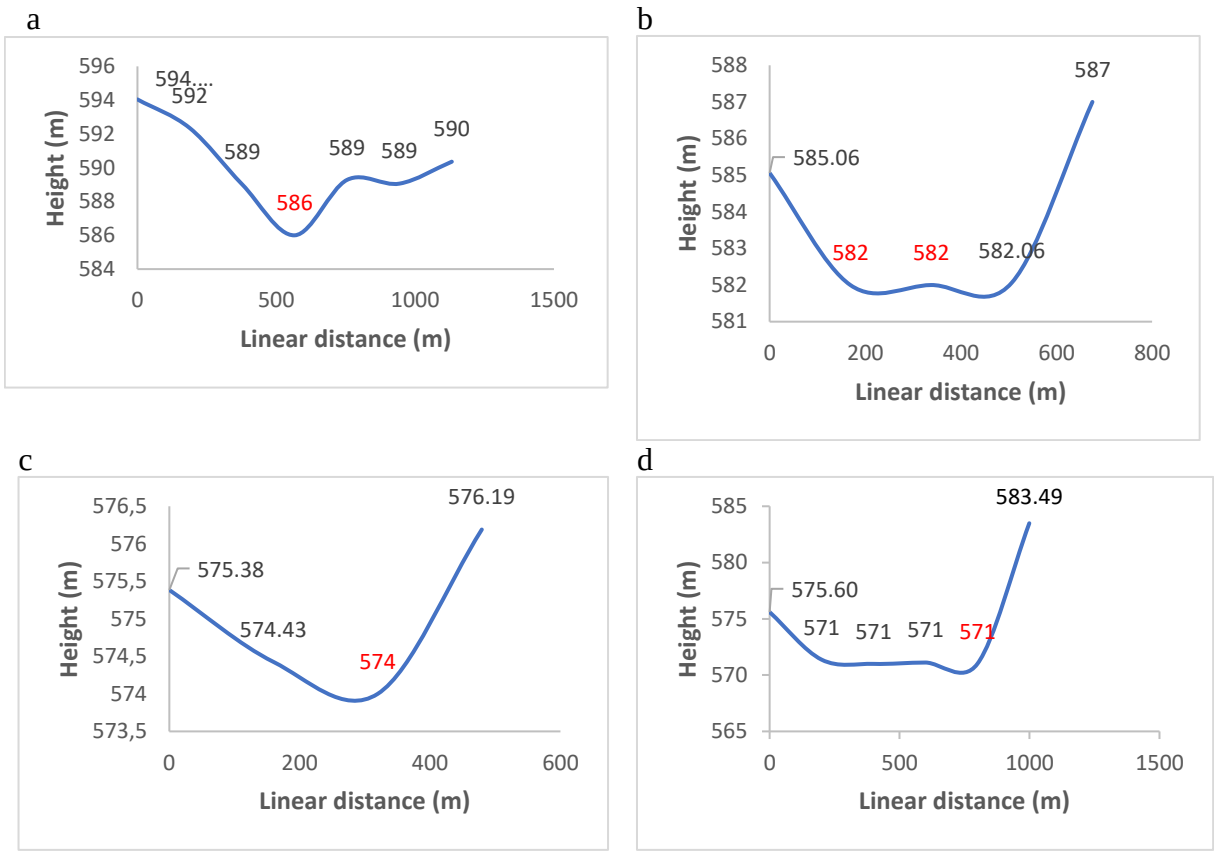

Figure 10: Cross-sections of regular channel of River-Kaduna at chainages: (a) 0+00 (b) 9+533 (c) 19+066 (d) 28+600.

The accuracy of the interpolated surface was evaluated by cross validation as stated earlier. Table 2 presents the descriptive statistics of the elevation errors for the TIN. The elevation difference in TIN interpolator ranged between 0 and 1.843m with a mean of 0.650 ±0.420m.

Table 2: Descriptive statistics of TIN validation

Variable	Min. (m)	Max. (m)	Mean (m)	MAE (m)	RMSE (m)	StDev (m)	Count
TIN	0	1.843	0.650	0.602	±0.806	±0.420	500

3.3 Flood Extent

The metrics of the "pre-flood" and "during-flood" are shown in Table 3. Figure 11 shows the "pre-flood" and the "during-flood" extents overlaid on Google image. The pre-flood, which is the regular river channel is shown in light blue color and is narrower, while the during-flood, which is the flooded month is shown in dark blue color and is broader (Figure 11). The pre-flood occupied a surface area of 2,748.16Km^2 with a volume of 17,804,379.17m^3. The during-flood also occupied a surface area of 15,603.37Km^2 with a volume of 218,565,875.21m^3. Therefore, the flood extent of the River was 12,855.2Km^2 and the volume is 200,761,496.04m^3. This infers that the River overtops its bank and flows into contiguous settlements.

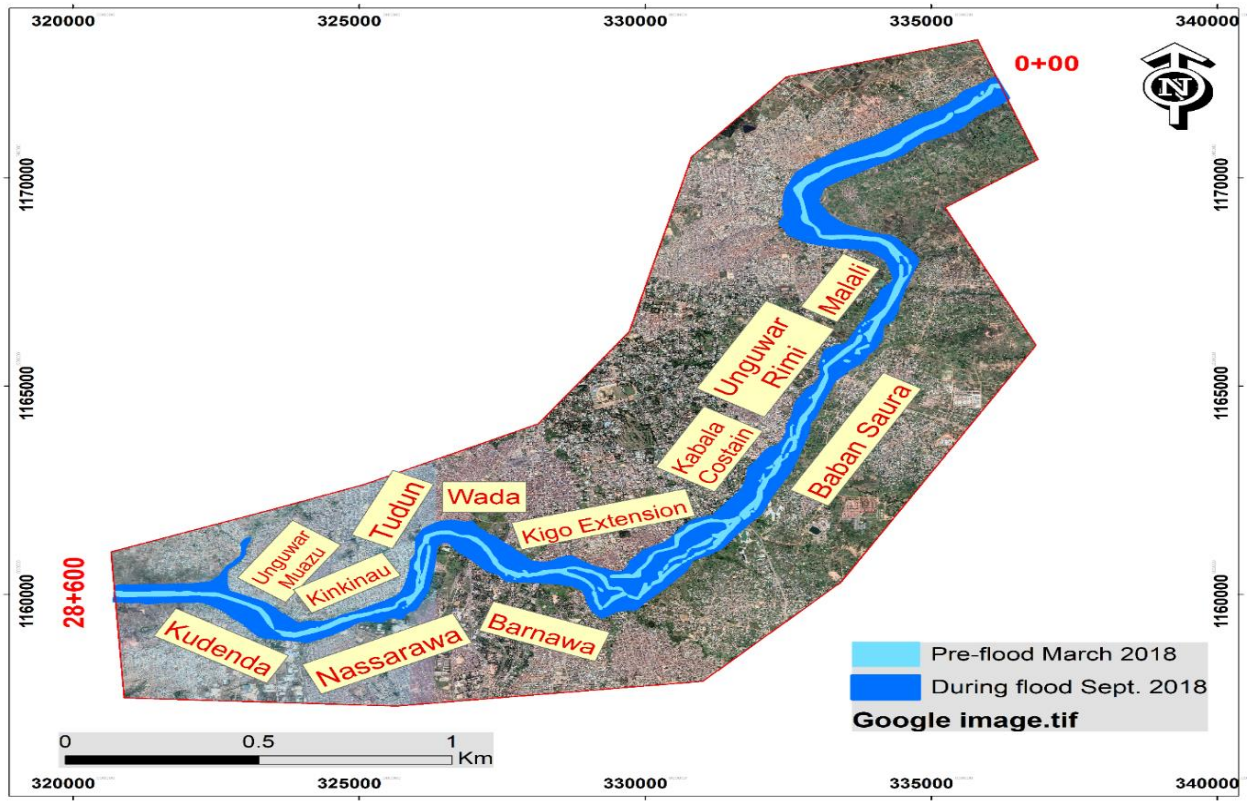

Figure 11: Flood extent of River-Kaduna.

Table 3: Metrics of Flood Extent of River-Kaduna

S/N	River State	Surface Area (Km^2)	Volume (m^3)
1	Pre-flood (March)	2,748.16	17,804,379.17
2	During-flood (September)	15,603.37	218,565,875.21
3	Flood extent (difference)	12,855.22	200,761,496.04

4. CONCLUSIONS AND RECOMMENDATIONS

This paper has mapped the extent of inundation along River-Kaduna using a simple, logical and effective method. The method is based on the integration of two sets of Landsat 8 (one acquired before and the other during the flood event) together with a DEM. The Landsat image provided a planimetric (extent) information and the DEM provided height information of the study area. Incorporating the DEM into the study helped in compensating for the unavailability of river gauge reading for the determination of the water level above the mean sea level. The profile of the River reveals that rock outcrops exits within the course of the River. The cross-section also reveals that the bank of the River at the right-hand side is lower than the bank on the left-hand side. It concluded that neighborhoods such as that lie in the right-hand side of the River are highly susceptible to inundation. Interestingly, the flow direction revealed the neighborhoods in the south, north, southwesterly, northwesterly, and northeasterly directions are highly susceptible to inundation. It revealed the area occupied by the water of the river channel before the flood and during the flood, together with their corresponding volumes.

It concluded that the River overtops its bank and flow into contiguous settlements. This study contributes to the strategy for mapping of extent of inundation in the absence of a river gauge data. This study will be a breakthrough for hydrological studies in ungauged areas.

From the findings of the study, it suggests that dredging should be carried out to allow the river to accommodate more volume of water during heavy rainfall and freely flow through its natural channel. Kaduna state government should endeavor to install river gauge to collect daily stages of the water level. This will help to monitor the water level and will serve as an early warning system. Also, the government should construct retaining walls at right bank of the River because of their lower elevation to protect neighborhoods along the right-hand side of the River.

ACKNOWLEDGEMENTS

The authors would like to acknowledge the U. S. Geological Survey for the provision of the Landsat imagery and the SRTMDEM datasets for this study.

REFERENCES

Akinola, A. K. (2015). A Review of Flood Risk Analysis in Nigeria. *American Journal of Environmental Science*, vol. 11 (3), 157-166. DOI: https://doi.org/10.3844/ajessp.2015.157.166.

Alayande, A N. and Agunwamba, J. C, (2010), The Impacts of Urbanization on Kaduna River Flooding, *Journal of American Science*, 6 (5), pp 28-35.

Amidon, W. (2014). *Dark Object Subtraction in ENVI*. [Video file). Retrieved from: https://www.youtube.com/watch?v=QYrglRO6JiY. Downloaded on: 5 December, 2020.

Chavez, P. S. (1988). An Improved Dark-Object Subtraction Technique for Atmospheric Scattering Correction of Multispectral Data. *Remote Sens Environ*; 24: 459–79.

Cwik, K. (2017). *Flood Mapping with the Sentinel-1 Time-Series Data in Arid Areas.* [Master Thesis – University of Munich]. Retrieved from: https://cartographymaster.eu/wp-content/theses/2017_CWIK_Thesis.pdf. Downloaded on: 28 November, 2020.

Daily Trust (2018). *Heavy Rainfall Causes Flash Flood in Kaduna*. [Online Newspaper]. Retrieved from: https://www.dailytrust.com.ng/heavy-rainfall-causes-flash-f…. Accessed on: 4 December, 2020.

Ejikeme, J. O., Igbokwe, J. I., Ojiako, J. C., Emengini, E. J. and Aweh, D. S. (2015). Modelling the Impact of Flooding using Geographic Information System and Remote Sensing. *International Journal of Technical Research and Applications*. Vol. 3 (4). Retrieved from: http://www.ijtra.com.

Elkhrachy, I. (2017). Vertical Accuracy Assessment for SRTM and ASTER Digital Elevation Models: A case study of Najran city, Saudi Arabia. *Ain Shams Engineering Journal*. doi:10.1016/j.asej.2017.01.007.

Environmental System for Research Institute (ESRI) (2016). *ArcGIS Desktop: Release Version: 10.5. Product Version: 10.5.0.6491*. Redlands, California, USA.

Environmental System for Research Institute (ESRI) (2016). *Elevation Void Fill Function.* ArcGIS Desktop Help File.

Gilmore, S., Saleem, A. and Dewan, A. (2015). *Effectiveness of DOS (Dark-Object Subtraction) Method and Water Index Techniques to Map Wetlands in a Rapidly Urbanizing Megacity with Landsat 8 Data*. In: Research@Locate'15. Brisbane; 10-12.

Geospatial Science (GSP) (2019). *GSP 216: Introduction to Remote Sensing: Radiometric Calibration and Corrections*. [Lecture Note – Humboldt State University]. Retrieved from: http://gsp.humboldt.edu/OLM/Courses/GSP_216_Online/lesson4-1/radiometric.html. Downloaded on: 4 December, 2020.

Habib, M., Alzubi, Y., Malkawi, A. and Awwad, M. (2020). Impact of Interpolation Techniques on the Accuracy of Large-Scale Digital Elevation Model. *Open Geosciences*, 12: 190-202. https://doi.org/10.1515/geo-2020-0012.

Huang, C. Chen, Y. Zhang, S and Wu, J. (2018). Detecting, Extracting, and Monitoring Surface Water from Space Using Optical Sensors: A Review. *Reviews of Geophysics.* https://doi.org/10.1029/2018RG000598.

Ijigah, E. A. and Akinyemi, T. A. (2015). Flood Disaster: An Empirical Survey of Causative Factors and Preventive Measures in Kaduna, Nigeria. *International Journal of Environment and Pollution Research,* vol. 3 (3): pp. 53-66.

Isioye, O. A., Combrinck, L. and Botai, J. (2015). Performance Evaluation of Blind Tropospheric Delay Correction Models over Africa. *South African Journal of Geomatics*, 4(4), 502-525–525. https://doi.org/10.4314/sajg.v4i4.10.

Islam, M. Z. (Undated). *Determination of Flood Extent Using Remote Sensing*. [A Term Paper – University of Alberta]. Retrieved from: https://sites.ualberta.ca/~mdzahidu/flood_mapping.pdf. Downloaded on: 28 November, 2020.

Isma'il, M. and Saanyol, I. O. (2013). Application of Remote Sensing (RS) and Geographic Information Systems (GIS) in flood vulnerability mapping: Case study of River Kaduna. *International Journal of Geomatics and Geosciences*, Vol. 3 (3): 0976 – 4380.

Jeb and Aggarwal, (2008). Flood Inundation Hazard Modelling of the River Kaduna Using Remote Sensing and Geographic Information Systems. *Journal of Applied Sciences Research*, 4 (12): 1822-1833.

Klemas, V. (2014). Remote Sensing of Floods and Flood-Prone Areas: An Overview. *Journal of Coastal Research*, 00(0), 000–. 000. Coconut Creek (Florida), 0749-0208.

Land Satellites Data System (LSDS) (2019). *Landsat 8 (L8) Data Users Handbook*. LSDS-1574 Version 5.0: November, 2019. Retrieved from: https://prd-wret.s3.us-west-2.amazonaws.com/assets/palladium/production/atoms/files/LSDS-1574_L8_Data_Users_Handbook-v5.0.pdf. Downloaded on: 2 December, 2020.

Lathrop, (2004). *Image Restoration and Atmospheric Correction*. Retrieved from: http://www.ssc.bibalex.org/viewer/detail.jsf;jsessionid. Downloaded on: 3 December, 2020.

Lawrence, M. K., Walker, N. D., Balasubramanian, S., Babin, A. and Baras, J. (2005). Applications of Radarsat-1 Synthetic Aperture Radar Imagery to Assess Hurricane-Related Flooding of Coastal Louisiana. *International Journal of Remote Sensing*, vol. 26 (24), 5359–5380.

Lisa, F., Ludtke, D. and Duguru, M. (Undated). *Capabilities of SAR and Optical Data for Rapid Mapping of Flooding Events*. Retrieved from: http://geomundus.org/2018/docs/papers/Lisa.pdf. Downloaded on: 28 November, 2020.

Miliaresis, G. C. and Paraschou, C. V. E. (2005). Vertical accuracy of the SRTM DTED level 1 of Crete. *Int J Appl Earth Obs Geoinf*; 7 (1): 49–59. URL http://www.sciencedirect.com/science/article/pii/S0303243405000024.

O'neil-Dunne, J. (2014). *Dark Object Subtraction*. [Video file). Retrieved from: https://www.youtube.com/watch?v=uXLzeTJG_to. Downloaded on: 5 December, 2020.

Premium Times (2018). *Flood Ravages three Kaduna LGAs*. [Online Newspaper]. Retrieved from: https://www.premiumtimesng.com/regional/nwest/281288-flood-ravages-three-kaduna-lgas.html. Accessed on: 4 December, 2020.

The Guardian (2020). *Flood Destroys Property in Kaduna Community*. [Online Newspaper]. Retrieved from: https://guardian.ng/news/flood-destroys-property-in-kaduna-community/. Accessed on: 4 December, 2020.

The Punch (2018). *Kaduna State warns Residents of Imminent Flooding*. [Online Newspaper]. Retrieved from: https://punchng.com/kaduna-state-warns-residents-of-imminent-flooding/. Accessed on: 4 December, 2020.

Wang, Y., Colby, J. D., and Mulcahy, K. A. (2002). An efficient method for mapping flood extent in a coastal floodplain using Landsat TM and DEM data, *International Journal of Remote Sensing*, vol. 23, no. 18, 3681–3696.

Xu, H. (2006). Modification of Normalized Difference Water Index (NDWI) to enhance open water features in remotely sensed imagery, *Int. J. Remote Sens*., 27 (14), 3025 –3033. http://dx.doi.org/10.1080/01431160600589179 IJSEDK 0143-11.

Yang, X. and Chen, L. (2017). Evaluation of Automated Urban Surface Water Extraction from Sentinel-2A Imagery Using Different Water Indices. *Journal of Applied Remote Sensing*, Vol. 11 (2): 026016. https://doi.org/10.1117/1.JRS.11.026016.

BIOGRAPHICAL NOTES

Abdulazeez Aliyu Onotu

Abdulazeez Aliyu Onotu is a lecturer in the Department of Geomatics at the Ahmadu Bello University Zaria, Nigeria, where he specializes in Earth Observation and Land Surveying. He has four (4) years' experience in lecturing and research. His researches are in the following subject areas: remotely sensed satellite image (visible, infrared and microwave) processing, mapping of flood extent, forestry, land degradation, crime incidents, Urban Heat Island (UHI), site suitability, utilities and infrastructure. He is currently working on precision agriculture for food security. Surveyor Aliyu is a member of some professional bodies including the National Association of Geodesy (NAG), National Association of Surveying & Geoinformatics Lecturers (NASGL), Surveyors' Council of Nigeria (SURCON), Nigerian Institution of Surveyors (NIS), FIG Young Surveyors Network (FIG YSN) and Northern Surveyors Forum (NSF). He has authored and co-authored over 10 articles.

Adamu Bala

Adamu Bala, is a Lecturer in the Department of Geomatics at the Ahmadu Bello University, Zaria, Nigeria, where he specializes in Geo-Information Science, Remote Sensing, Mining Surveying and Professional Practice. He obtained B.Eng. & MSc. Geomatics; PGDE; PGD Mining Enginnering and currently enrolled for PhD. Geomatics. He had previously worked with Kabir & Associates Limited, Katsina and Nigerian Institute of Mining and Geosciences, Jos as Surveyor/GIS Analyst and Geoscientist respectively for cumulative 7 years, before joining Academia in 2018. Surveyor Bala is Registered/Licensed as a Surveyor with the Surveyors Council of Nigeria and a member of some professional bodies including the Nigerian Institution of Surveyors (NIS), FIG Young Surveyors Network (YSN), Nigeria, National Association of Surveying & Geoinformatics Lecturers (NASGL), Northern Surveyors Forum (NSF), amongst others. He has attended and fully participated at numerous national and international Conferences including FIG Working Week, 2013 in Abuja; and has numerous local and international publications to his credit.

AbdulHameed Isiaka Usman

Abdulhameed Isiaka Usman is a lecturer in the Department of Surveying and Geoinformatics at Waziri Umaru Federal Polytechnic, Birnin Kebbi, NIgeria, where he specializes in Geo-informatics. He has 5 years' experience in lecturing and as an analyst in the mapping of infrastructure and utilities, Geospatial analysis of health-related issues and geographical information system for sustainable development. He is a member of some professional bodies including the National Association of Surveying and Geoinformatics Lecturers (NASGL), Northern Surveyors Forum (NSF), Nigeria Institution of Surveyors (NIS) and FIG Young Surveyors Network (YSN). He has authored and co-authored over five (5) articles both in conferences and Journal.

Zenabu Attah Kaka

Zenabu Attah Kaka is a Lecturer in the Department of Geomatics at the Ahmadu Bello University Zaria, Kaduna State Nigeria, where she specializes in Geographical Information System (GIS), image processing, Geo-positioning, Land Surveying and Engineering and Infrastructural Design. She is currently running her PhD in suitability mapping of electoral polling units. She has gained years of' experience in surveying and Geomatics from Lord'sfield Ltd in Lagos, Polaris Digitech Lagos, Nigeria Prison Services Akure, Cheth Consults Abuja, Folis Consults Abuja and Shemomal Nigeria Ltd Abuja. Surv. Kaka is registered with the Surveyor Council of Nigeria (SURCON) and also a member with the Nigeria Institution of Surveyors (NIS), National Association of Surveying & Geoinformatics Lecturers (NASGL), Women in Surveying (WIS), FIG Young Surveyors Network (FIG YSN), Surveyors Wives Association of Nigeria (SWAN), Geoinformation Society of Nigeria (GEOSON).

Muhammad Tijjani Kareto

Muhammad Tijjani Kareto recently graduated from the Department of Geomatics at the Ahmadu Bello University, Zaria, Nigeria, where he did his final year project in Geographical Information System (GIS) and Remote Sensing. He has flair for GIS related analyses. He is

currently doing his mandatory community service of National Youth Service Corps (NYSC). He is a, FIG Young Surveyors Network (YSN) and Northern Surveyors Forum (NSF).

CONTACTS

Mr AbdulAzeez Aliyu
Ahmadu Bello University
Sokoto Road, Samaru
Zaria
NIGERIA
Tel. +2348024398485
Email: abdulonotu@gmail.com; aoaliyu@abu.edu.ng
Web site: www.abu.edu.ng

Surv. Adamu Bala
Ahmadu Bello University
Sokoto Road, Samaru,
Zaria
NIGERIA
Tel. +2348065651016
Email: adambala09@yahoo.com; abala@abu.edu.ng
Web site: www.abu.edu.ng

Mr Abdulhameed Usman Isiaka
Waziri Umaru Federal Polytechnic, Birnin Kebbi
Kebbi State, Nigeria
Tel. +2347035601702
Email: usmanabdulhameed85@gmail.com
Web site: https://www.wufpbk.edu.ng/

Surv. Zenabu Atta Kaka
Ahmadu Bello University
Sokoto Road, Samaru
Zaria
NIGERIA
Tel. +2348033733784
Email: kakaattaz@gmail.com; zkatta@abu.edu.ng
Web site: www.abu.edu.ng

Mr Muhammad Tijjani Kareto
Ahmadu Bello University
Sokoto Road, Samaru
Zaria.
NIGERIA

Tel. +2349066216364
Email: muhammadtijjani534@gmail.com
Web site: www.abu.edu.ng